ACS Chemical Neuroscience

Research Article

pubs.acs.org/chemneuro

Structures and Free Energy Landscapes of the Wild-Type and A30P Mutant-Type α-Synuclein Proteins with Dynamics

Olivia Wise-Scira,[†] Ahmet Kemal Aloglu,[†] Aquila Dunn,[†] Isin Tuna Sakallioglu,[§] and Orkid Coskuner*[,†,‡]

[†]Department of Chemistry and [‡]Neurosciences Institute, The University of Texas at San Antonio, One UTSA Circle, San Antonio, Texas 78249, United States

[§]Department of Chemistry, Bilkent University, Ankara, Turkey 06800 and

Supporting Information

ABSTRACT: The genetic missense A30P mutation of the wild-type α-synuclein protein results in the replacement of the 30th amino acid residue from alanine (Ala) to proline (Pro) and was initially found in the members of a German family who developed Parkinson's disease. Even though the structures of these proteins have been measured before, detailed understanding about the structures and their relationships with free energy landscapes is lacking, which is of interest to provide insights into the pathogenic mechanism of Parkinson's disease. We report the secondary and tertiary structures and conformational free energy landscapes of the wild-type and A30P mutant-type α-synuclein proteins in an aqueous solution environment via extensive parallel tempering molecular dynamics simulations along with thermodynamic calculations. In addition, we present the residual secondary structure component transition stabilities at the atomic level with dynamics in terms of free energy change calculations using a new strategy that we reported most recently. Our studies yield new interesting results; for instance, we find that the A30P mutation has local as well as long-range effects on the structural properties of the wild-type α-synuclein protein. The helical content at Ala18-Gly31 is less prominent in comparison to the wild-type α-synuclein protein. The β-sheet structure abundance decreases in the N-terminal region upon A30P mutation of the wild-type α-synuclein, whereas the NAC and C-terminal regions possess larger tendencies for β-sheet structure formation. Long-range intramolecular protein interactions are less abundant upon A30P mutation, especially between the NAC and C-terminal regions, which is linked to the less compact and less stable structures of the A30P mutant-type rather than the wild-type α-synuclein protein. Results including the usage of our new strategy for secondary structure transition stabilities show that the A30P mutant-type α-synuclein tendency toward aggregation is higher than the wild-type α-synuclein but we also find that the C-terminal and NAC regions of the A30P mutant-type α-synuclein are reactive toward fibrillzation and aggregation based on atomic level studies with dynamics in an aqueous solution environment. Therefore, we propose that small molecules or drugs blocking the specific residues, which we report herein, located in the NAC- and C-terminal regions of the A30P mutant-type α-synuclein protein might help to reduce the toxicity of the A30P mutant-type α-synuclein protein.

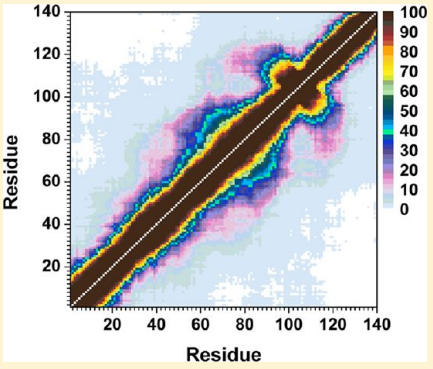

KEYWORDS: *α-Synuclein, genetic missense mutation, free energy landscape, molecular dynamics simulations*

The α-synuclein (αS) protein is a 140 amino acid residue intrinsically disordered fibrillogenic protein that is the main component of the large aggregates, termed Lewy bodies, which are a pathological hallmark of Parkinson's disease as well as other neurodegenerative disorders.[1−6] Genetic variants involving either a missense mutation or triplication of the gene for the αS protein have been isolated in familial forms of Parkinson's disease.[7−10] For example, a genetic missense mutation that results in the mutation of the Ala30 residue to a Pro residue, or the A30P mutation, was initially found in the members of a German family who developed Parkinson's disease.[8] The exact role of αS in the disease mechanism remains poorly understood, partially due to the difficulties associated with measuring the structures of intrinsically disordered fibrillogenic proteins at the monomeric and oligomeric levels. Monomeric and oligomeric forms of intrinsically disordered fibrillogenic proteins determine the aggregation mechanism.[11,12] Furthermore, the monomeric and oligomeric forms of αS are proposed to be the neurotoxic species in the pathogenic mechanism of Parkinson's disease due to the crucial role of their structural properties in the aggregation process.[13,14] However, studies performed with conventional tools face challenges in the measurements of monomeric αS protein structures due to fast aggregation, rapid conformational changes, and solvent effects. Besides these difficulties, detailed understanding of the structures and conformational free energy landscapes of the wild-type and A30P mutant-type αS proteins in solution can provide the currently missing detailed knowledge about the effect of the A30P genetic missense mutation on the αS protein, which in turn furnishes the

Received: November 5, 2012
Accepted: January 14, 2013
Published: January 14, 2013

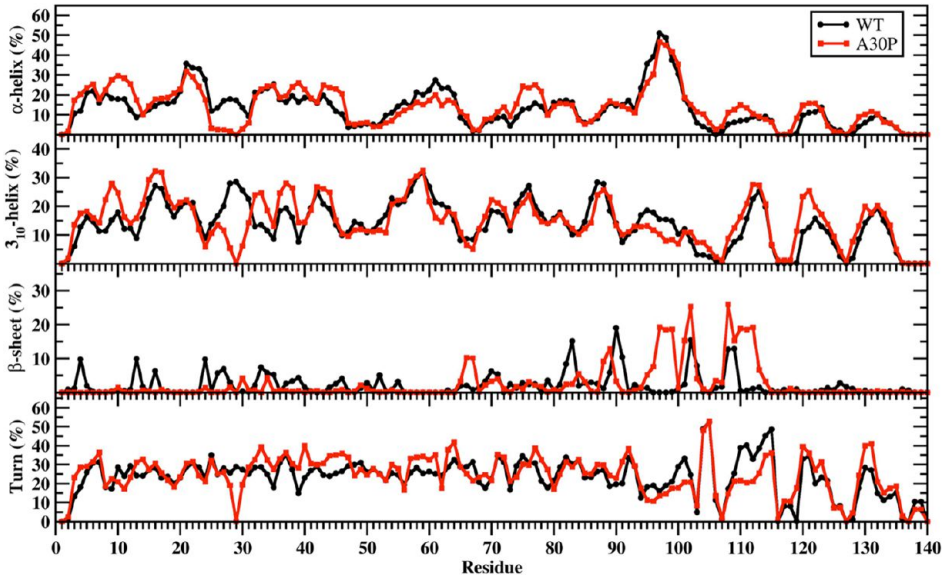

Figure 1. Wild-type and A30P mutant-type αS secondary structure components. Secondary structure component abundances per residue for the wild-type (black) and A30P mutant-type (red) αS structures obtained after convergence. The abundances for the π-helix and coil structures are not displayed.

required information for gaining more insights into the disease mechanism and designing more efficient treatments.

Interestingly, the current literature involves a debate about the structural properties of the A30P mutant-type αS protein. It was reported that the fibril structure of the A30P mutant-type αS is similar to that of the wild-type αS protein.[14−19] Despite this, the aggregation kinetics, neurotoxicity, and oligomeric structural properties of the wild-type αS were shown to be affected by the A30P mutation. Specifically, various experimental studies have reported that the A30P mutation results in an increase in the rate of oligomerization and aggregation of αS while the rate of fibril formation is decreased in comparison to the wild-type αS.[11,12,14,15,20−23] However, Ono et al. reported that the A30P mutation decelerates the rate of oligomerization.[24] The A30P mutant-type αS is also reported to be more neurotoxic than the wild-type αS, which has been linked to the reported increased oligomerization rate upon A30P mutation.[23,25−27] Even though far-ultraviolet-circular dichroism (far-UV-CD) measurements do not reveal secondary structural differences between the wild- and mutant-type αS proteins,[12,15] various other measurements have presented that the conformational behavior of A30P mutant-type αS differs from that of the wild-type αS protein. Bertoncini et al. reported via nuclear magnetic resonance (NMR) measurements that the long-range interactions of the A30P mutant-type αS are reduced in comparison to the wild-type αS protein.[28] Furthermore, it was shown that the A30P mutation affects the formation of helical structure around the location of the mutation.[28,29] An increase in β-sheet conformation was observed for αS upon A30P mutation by single molecule force (SMF) and Fourier transform infrared (FTIR) spectroscopies.[11,12,30] Utilizing far-UV-CD and Förster resonance energy transfer (FRET) measurements, Deniz and co-workers demonstrated that the folding landscape of the αS protein in the presence of sodium dodoceyl sulfate (SDS) is shifted from a three-state to a two-state transition upon A30P mutation.[31] In addition, the interaction of αS with lipid vesicles and membranes was shown to be less abundant in the A30P mutant-type αS monomer in comparison to its oligomeric state.[13,32]

Theoretical studies can complement experiments and provide structural and thermodynamic information at the atomic level with dynamics. For example, recent successful studies by Carloni and co-workers reported various structural properties; average distance between residues, radius of gyration and structural flexibility of the wild-type and A53T mutant-type human αS and wild-type mouse αS obtained from molecular dynamics (MD) simulations using an explicit model for water.[33] Yet, the secondary structural properties per residue of these three αS proteins were not reported in this study. Furthermore, the impacts of the confined aqueous volume effect on the reported results are unknown. Moreover, Chatterjee et al. reported transient decreases to the helical structure around the mutation site in the A30P mutant-type αS via classical MD simulations.[34] However, MD simulations without the usage of special sampling techniques face limitations in configurational sampling of the full-length intrinsically disordered fibrillogenic proteins that lack a stable structure and suffer from the multiple minima problem. Furthermore, the variations in the secondary and tertiary structures as well as free energy landscapes were not presented in these earlier studies. Annealing molecular dynamics simulations by Balesh et al. presented a decrease in α-helix structure in the A30P mutant-type αS protein structures but an increase in the 3$_{10}$-helix abundance and no change in the β-sheet structure formation upon A30P mutation of the wild-type αS.[35] Detailed information about the tertiary structure and conformational free energy landscape differences was not reported. Furthermore, Perlmutter et al. demonstrated successfully that the destabilization of the secondary structure around the mutation site in the A30P mutant-type αS decreased interactions with a micelle via MD simulations without the usage of special sampling techniques.[36] In addition, Kumar et al.[60] performed classical MD simulations on the structures of the wild-type and A30P mutant-type αS proteins. Even though interesting information was presented, the secondary and tertiary structures of the A30P mutant-type protein were not discussed in their study.

To the best of our knowledge, an in depth, atomic-level comparison of the impact of the A30P mutation on the structural and thermodynamic properties of the wild-type αS protein in aqueous solution that includes secondary and tertiary structures as well as the dependence of these properties on the free energy landscapes has not yet been presented in the literature. In this study, we compare the secondary and tertiary structural properties as well as the free energy landscapes of the wild-type and A30P mutant-type αS proteins in an aqueous solution environment at the atomic level with dynamics. We also studied the secondary structure transition stabilities at the atomic level with dynamics using our in-house developed method that we presented most recently. To achieve these results, we have performed extensive all-atom parallel tempering MD simulations, which is one type of special sampling technique that enhances conformational sampling of protein structures, on the full-length wild-type and A30P mutant-type αS proteins. From these simulations, we have obtained interesting trends in the secondary and tertiary structural properties and thermodynamic preferences of the wild-type and A30P mutant-type αS that provide insight into the proposed differences in aggregation kinetics of these two proteins. We also investigated the potential of mean force (PMF) surfaces of these two proteins, which we previous applied successfully on the wild-type and mutant-type amyloid-β proteins in the vicinity and absence of cofactors.[37−39] Additionally, the application of our newly in house developed theoretical strategy and software package (ProtMet), which we presented most recently, has enabled insights into the dynamic stabilities between secondary structure component conversions per residue in an aqueous solution medium.[39,40]

RESULTS AND DISCUSSION

Figure 1 presents the calculated residual secondary structure components with dynamics of the wild-type and A30P mutant-type αS proteins in an aqueous solution medium. The helical and β-sheet structure formations have been proposed to play crucial roles in the aggregation process of intrinsically disordered fibrillogenic proteins at the center of neurodegenerative diseases.[12,14,24,41] Within the N-terminal region (Met1-Lys60) of the wild-type and A30P mutant-type αS, we detect abundant α-helix formation at Ala19-Lys23 and 3_{10}-helix formation at Val15-Ala18, Glu20-Thr22, Gly41-Thr44, and Thr54-Lys60 varying between 20% and 35% (Figure 1). Interestingly, Gly7-Glu13, Val15-Ala17, Lys32-Val40, and Lys43-Gly47 adopt more prominent helical structure (α-helix or 3_{10}-helix; up to 30%) in the structures of the A30P mutant-type than in those of the wild-type αS protein. In contrast, the α-helix and 3_{10}-helix contents at Gly25-Lys32 in the wild-type αS protein structures decrease or disappear upon A30P mutation. This finding is in agreement with the NMR measurements that reported reduced helical propensity for Ala18-Gly31 upon A30P mutation.[28,29] Moreover, our results are in partial agreement with those of Chatterjee and Sengupta, who presented a decrease in helix abundance around the mutation site of the A30P mutant-type αS in comparison to the wild-type αS, by MD simulations.[34] Bussell and Eliezer proposed that destabilization of helix formation in this region may be associated with the increased rate of oligomerization of the A30P mutant-type rather than wild-type αS.[29] Consequently, our results suggest an increase in oligomerization rate of the A30P mutant-type αS in comparison to the wild-type. We detect abundant helical structure formation (>20%) in the nonamyloid β component region (NAC; Glu61-Val95) at Glu61-Val63, Thr75-Gln79, and Ser87-Ala89 in the conformations of the wild-type and the A30P mutant-type αS proteins. Furthermore, the α-helical content at Thr75-Gln79 is up to 9% larger in the structures of A30P mutant-type rather than wild-type αS. However, the 3_{10}-helix abundance at Glu61-Gln62 decreases (up to 30%) upon A30P mutation of the wild-type αS protein. The α-helix abundance in the C-terminal region is similar for both wild-type and A30P mutant-type αS, with the highest abundance observed at Lys96-Gly101. Nevertheless, we do observe more abundant α-helix formation at Pro108-Ile112 in the A30P mutant-type structures in comparison to the wild-type αS structures in an aqueous solution environment. In addition, Gly111-Glu114 and Gly132 located in the C-terminal region present abundant 3_{10}-helix formation (up to 28%) for both the wild-type and A30 mutant-type αS proteins. We also note a larger decrease in 3_{10}-helix abundance (≥5%) at Phe94-Leu100 in the A30P mutant-type structures rather than those of the wild-type αS protein.

Abundant β-sheet structures (5% to 20%) are formed in parts of the NAC and C-terminal regions (Val70, Val71, Val82, Glu83, Ala89-Ala91, Lys102, Asn103, Pro108, and Gln109) in the structures of the wild-type αS protein. A similar trend is observed for the A30P mutant-type αS structures with a significant increase in β-sheet formation at Val66, Gly67, Ile88, Ala89, Val95-Gln99, Gly101, Lys102, and Pro108-Glu114. These findings support previous NMR measurements that reported β-sheet structure in the C-terminal region of both the wild- and A30P mutant-type αS proteins.[29] Furthermore, SMF and FTIR spectroscopic measurements reported increased β-sheet conformation for the A30P mutant-type αS structures in comparison to those of the wild-type αS protein structures.[11,12,30] In contrast to our findings, previous annealing MD simulations performed by Balesh et al. did not show an increase in β-sheet formation in the A30P mutant-type αS structures in comparison to those of the wild-type αS protein.[35] Additionally, we find that the N-terminal region possesses abundant β-sheet structure (≥5% probability) at Phe4, Glu13, Val16, Gln24, Val26, Ala27, Thr33-Glu35, and Val37 in the wild-type αS conformations that disappears in the structures of the A30P mutant-type αS protein. This result supports the NMR measurements performed by Bussell and Eliezer, who suggested a possible decrease in β-sheet formation upon A30P mutation in the N-terminal region of the wild-type αS protein.[29] We also note that β-sheet abundance decreases at Val82, Glu83, Ala90 and Ala91 upon A30P mutation of the wild-type αS protein. As mentioned above, β-sheet structure formation has been linked to the aggregation process.[11,12,14] Therefore, and based on our findings, the N-terminal region of A30P mutant-type αS is less likely to participate in the aggregation process than the same region in the wild-type αS protein. Furthermore, our results predict that the C-terminal region and part of the NAC region of A30P mutant-type αS are more reactive toward aggregation than the same regions in the wild-type αS protein. These findings support the experimental findings that report a faster rate of oligomer formation for the A30P mutant-type αS in comparison to the wild-type.[11,12,14,15,20−23] We should mention here again that β-sheet formation is associated with the self-association and aggregation of αS, including the formation of dimeric, oligomeric, and fibril structures.[11,12,14] Furthermore, β-sheet formation in the NAC region was proposed to play an important role in the intermolecular interactions between the

dx.doi.org/10.1021/cn300198q | ACS Chem. Neurosci. 2013, 4, 486−497

monomeric species.[29] Therefore, the increased β-sheet structure formation in the NAC and C-terminal regions that we find upon A30P mutation may be associated with the reported larger oligomerization rate that was detected for the A30P mutant-type oligomers. The N-terminal region and β-sheet formation in this region was also proposed to be crucial in fibril formation, yet we detect a decrease in β-sheet formation in the N-terminal region, which indicates rather an inhibition of fibril formation via the N-terminal region.[17,29,42,43] Abundant (up to 55%) turn structure formation occurs in the C-terminal region of the wild- and A30P mutant-type αS proteins. Large decreases in the tendencies toward turn structure formation occur in the N-terminal region at Glu28-Pro30 and in the C-terminal region (Gln109-Asp115) with a difference up to 30%. However, turn structure abundance is increased at Thr33, Val40, Thr44-Gly47, Glu57-Glu61, Val63, Thr64, Glu130, and Glu131 ($\geq$5%) upon A30P mutation of the wild-type αS protein.

In addition to determining the abundance of the formation of specific secondary structure components, we also calculated the free energy change values for the transitions between two different secondary structure components for each residue of the wild-type and A30P mutant-type αS proteins (Figure 2) using our recently developed theoretical strategy.[39,40] The free energy values identify which secondary structure transitions are most preferred and thus can be used to identify which structures are most likely to precede the formation of secondary structure components of interest. These calculations show turn or helix to coil transitions as well as helix to turn or turn to helix transitions are overall the most preferred secondary structure transitions for both the wild-type and A30P mutant-type αS proteins in an aqueous solution environment. Due to the proposed importance of helical and β-sheet structures in the aggregation mechanism of αS proteins, the transitions to and from these structures are of particular interest. In the N-terminal region, transitions from turn to helix structures are the most preferred at Val3-Lys60 in the wild-type αS protein (Figure 2, top). Even though transitions to a β-sheet structure are generally less preferred than transitions to helical structure in the N-terminal region of the wild-type αS, we do note that coil to β-sheet transitions present the same thermodynamic preference as turn to helix and coil to helix transitions for residues Phe4 and Glu13. Upon A30P mutation of the wild-type αS, the thermodynamic stability of transitions to a helix structure from any other secondary structure (turn, coil or β-sheet) at Gln24-Gly31 decreases (Figure 2, bottom). Instead, we observe an increase in preference for turn to coil transitions for these residues. Furthermore, Pro30 shows an increase in preference for transitions to a β-sheet structure in comparison to the Ala30 residue of the wild-type αS. In contrast, the remaining residues of the N-terminal region present a decreased thermodynamic preference for all transitions to a β-sheet structure. Turn to helix transition is also most preferred in the NAC region of both the wild-type and A30P mutant-type αS proteins. Additionally, coil to β-sheet transitions present a similar thermodynamic preference as the turn to helix transitions for residues Ala90 and Ala91 in the wild-type αS and residues Val66, Gly67, and Ala89 in the A30P mutant-type αS. In the C-terminal region, turn to coil transition is the most stable overall. However, specific residues in the C-terminal region display different preferred secondary structure component transitions. For example, turn to helix transition is the most stable conversion at Lys96-Lys102 for both the wild- and

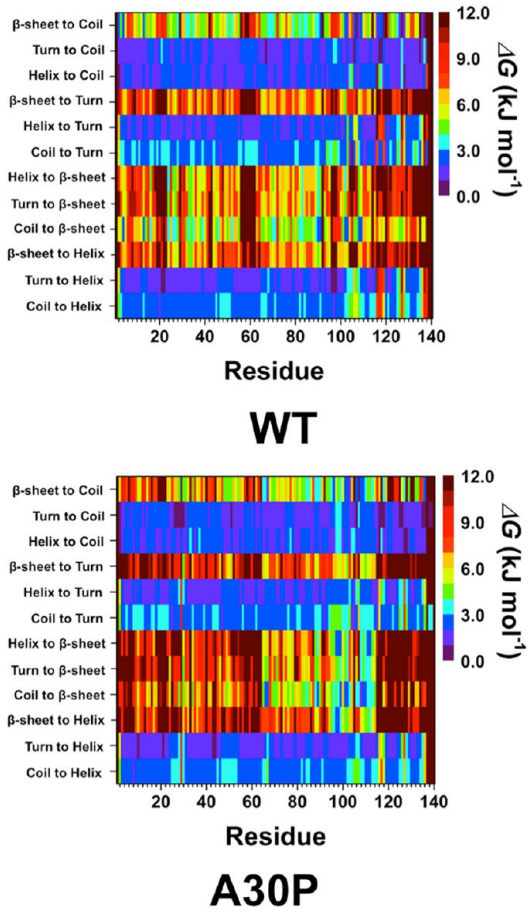

Figure 2. Wild-type and A30P mutant-type αS secondary structure transition stabilities. The stability of secondary structure transitions between two specific secondary structure components per residue for the wild-type (WT) and A30P mutant-type (A30P) αS proteins based on extensive Gibbs free energy calculations performed using our recently developed theoretical strategy. The color scale corresponds to the free energy value associated with the specific secondary structure transition between two secondary structure components for a specific residue.

mutant-type proteins. Turn or coil to helix as well as helix to turn secondary structure transitions are not preferred at Met116-Asp199 in the wild-type αS protein. Yet, the thermodynamic stability of these transitions increases upon A30P mutation of αS for the same residues. We also note that coil to β-sheet transition is preferred at Lys102, Asn103, Pro108, and Gln109 in the C-terminal region of the wild-type αS. In the A30P mutant-type αS, coil to β-sheet transitions are preferred at Gln99, Gly101, Lys102, and Pro108-Glu110. In addition, stable helix to β-sheet transition is detected at Lys97-Gln99, Gly111, and Ile112; stable β-sheet to helix transition occurs at Lys97 and Asp98. We also note an overall increase in the preference of bisecondary structure component transitions resulting in the formation of a β-sheet structure as well as β-sheet to helix transition at Lys96-Glu114 upon A30P mutation of the wild-type αS protein. In contrast, a vice versa trend occurs for residues located at Asp115-Ala140 in the C-terminal region. Overall, these findings are in agreement with NMR measurements that are described above but provide in-depth insights into the residual bisecondary structure transition stabilities that are currently not assessable experimentally using conventional tools.

dx.doi.org/10.1021/cn300198q | ACS Chem. Neurosci. 2013, 4, 486−497

The calculated intramolecular protein interactions in the structures of the wild-type and A30P mutant-type αS proteins are presented in Figure 3. We detect strong intramolecular

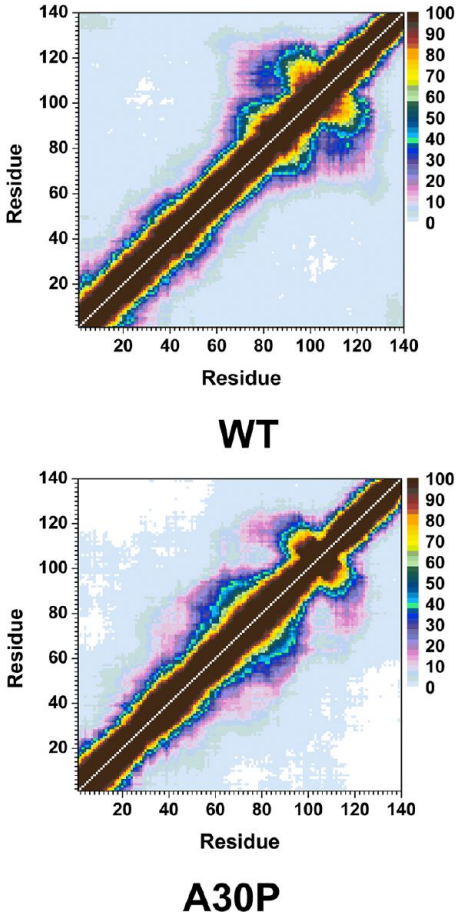

Figure 3. Wild-type and A30P mutant-type αS tertiary structures. Calculated intramolecular interactions of the wild-type (WT) and the A30P mutant-type (A30P) αS. The color scale corresponds to the probability (*P*) of the distance between the heavy atoms (C, N, O, S) of a residue being ≤20 Å from each other.

interactions between Gly86-Asn103 in the NAC region and Glu104-Asn122 in the C-terminal region with an abundance larger than 50% in the structures of the wild-type αS protein (Figure 3, top). Furthermore, Val70-Gly84 and Ala85-Leu100 in the NAC region of the wild-type αS protein present strong intramolecular interactions (up to 90%). We also note prominent interactions between Ala56-Gly106 and Gly84-Gln134 (up to 40%). Thus, we find moderate interactions between the N-terminal, NAC and C-terminal regions with the NAC and C-terminal regions. Overall, these tertiary structure findings agree with the previous theoretical studies performed by Carloni and co-workers.[33] Interestingly, the intramolecular interactions in the structures of the wild-type αS are significantly influenced by the A30P mutation (Figure 3, bottom). Even though some intramolecular interactions between a part of the NAC region (Ile88-Asn103) and the C-terminal region (Glu104-Pro120) occur, the abundances of these interactions are decreased in the A30P mutant-type αS in comparison to the wild-type αS structures. Moreover, abundant (up to 40%) intramolecular interactions occur between Lys58-Val95 and the C-terminal region (Lys96-Pro128). Intramolecular interactions between the N-terminal region (Val26-Lys58) and the NAC and C-terminal regions (Gln62-Leu100) are also detected. However, intramolecular interactions between the N-terminal region (Met1-Lys60) and Val118-Val140 of the C-terminal region disappear upon A30P mutation of the wild-type αS monomer in an aqueous solution medium. Similar trends are also detected for the intramolecular interactions between residues Met1-Val16 of the N-terminal region and the NAC region. This finding along with the decreased intramolecular interactions between the NAC and C-terminal regions of the A30P mutant-type αS presents that the NAC region is more solvent exposed in the A30P mutant-type rather than in the structures of the wild-type αS protein. The reduced long-range intramolecular interactions as well as the increased exposure of the NAC region upon A30P mutation of the wild-type αS protein agree with some previous NMR measurements of the wild-type and A30P mutant-type αS.[28] Furthermore, the less abundant long-range interactions and increased exposure of the NAC region have been proposed to potentiate the aggregation of the wild-type αS protein by allowing the NAC region, which is proposed to be a key in the fibrillogenesis process, to be more available for intermolecular interactions with surrounding monomers rather than intramolecular interactions.[28,44,45] Therefore, our tertiary structure findings along with our secondary structure property investigations present that the A30P mutant-type αS protein tends to be more reactive toward aggregation than the wild-type αS, which is in agreement with some experimental measurements.[11,12,14,20−22] Time-resolved fluorescence energy-transfer measurements reported an increased donor to acceptor distance upon A30P mutation of αS, which agrees with our less compact structure of A30P mutant-type αS in comparison to the wild-type αS.[46] The same trend is also obtained in the probability distribution of the radius of gyration (R_g) for both proteins (Figure 4). Specifically, the probability of the

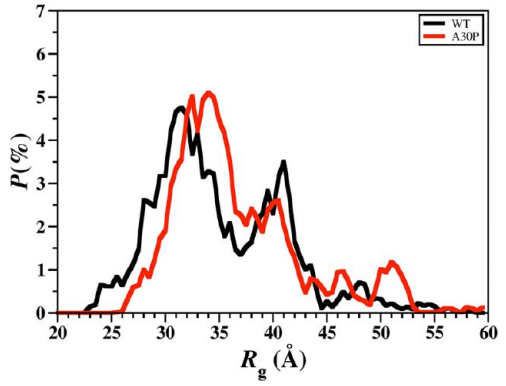

Figure 4. Wild-type and A30P mutant-type αS radius of gyration values. The probability distribution of the radius of gyration (R_g) values of the wild-type (black) and A30P mutant-type (red) αS for the structures obtained after convergence.

structures with an R_g value between 22.3 Å and 31.8 Å is larger for the wild-type than the A30P mutant-type αS structures, whereas, the vice versa trend is obtained for R_g values varying between 31.0 and 38.3 Å. Although the wild-type structures present a slightly higher probability for structures with R_g values varying between 38.8 and 43.8 Å and between 47.4 and 48.9 Å than the A30P mutant-type αS, the opposite trend is detected for R_g values larger than 44.0 Å. NMR

dx.doi.org/10.1021/cn300198q | ACS Chem. Neurosci. 2013, 4, 486−497

Table 1. Calculated average enthalpy (H), solvation free energy (G_{sol}), $H-G_{sol}$, Entropy (TS), and Gibbs Free Energy (G) Values for the Wild-Type (WT) and A30P Mutant-Type (A30P) α-Synuclein Proteins

peptide	$\langle E_{total} \rangle$ (kJ mol^{-1})	$\langle G_{sol} \rangle$ (kJ mol^{-1})	$\langle H \rangle$ (kJ mol^{-1})	$T\langle S \rangle$ (kJ mol^{-1})	$\langle G \rangle$ (kJ mol^{-1})
WT	7146.5 (±174.3)	−16 704.1 (±169.7)	−9557.4 (±18.4)	7043.8 (±8.4)	−16 601.4 (±13.0)
A30P	7861.6 (±240.8)	−17 323.0 (±200.0)	−9461.4 (±50.8)	7057.3 (±18.8)	−16 518.7 (±32.1)

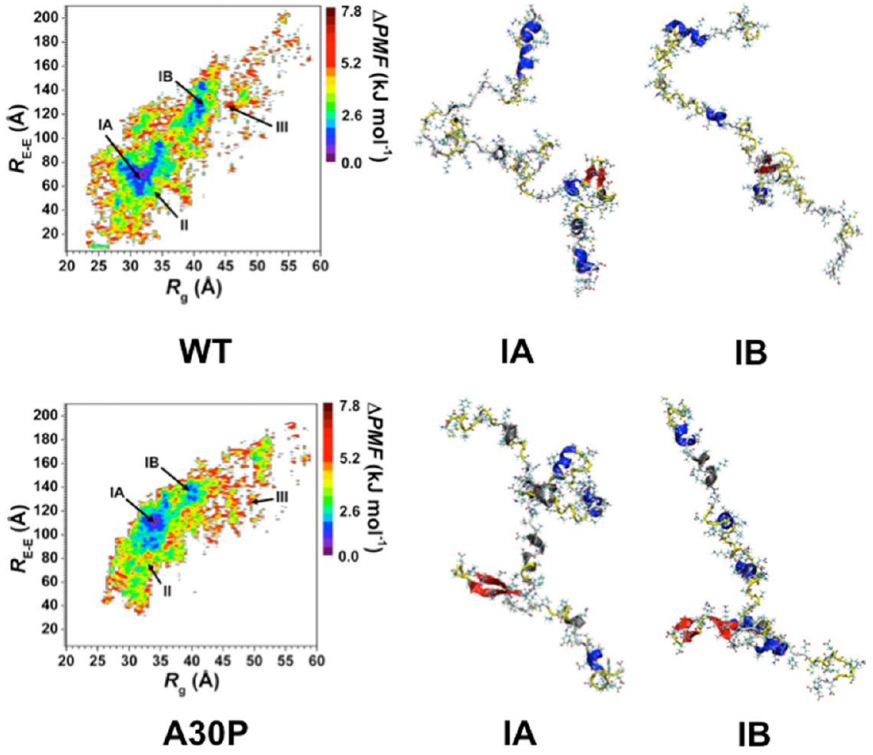

Figure 5. Wild-type and A30P mutant-type αS PMF surfaces. Change in the potential of mean force (ΔPMF) of the wild-type (WT) and A30P mutant-type (A30P) αS along the coordinates of radius of gyrations (R_g) and end-to-end distance ($R_{E\text{-}E}$) in units of kJ mol^{-1}. The reference value for the PMF surfaces are 6.73 and 6.48 kJ mol^{-1} for the wild-type and A30P mutant-type αS, respectively.

measurements also predicted a decrease in long-range interactions in the structures of the A30P mutant-type αS rather than the wild-type αS protein, which agrees overall with our observed decreased compactness of the wild-type αS protein upon A30P mutation.[28] We also note that the probability distribution of R_g values of the wild-type αS agrees with the range of R_g values reported by previous theoretical studies by Losasso et al.[33]

The thermodynamic values, specifically the conformational Gibbs free energy values (G) including conformational enthalpic (H) and entropic (TS) contributions, for the structures of the wild-type and A30P mutant-type αS proteins are presented in Table 1. The conformational Gibbs free energy provides a quantitative estimate of the relative stability of the wild-type and A30P mutant-type αS structures in aqueous solution. Based on the difference in conformational Gibbs free energy values, the structures of the wild-type αS protein are more stable by 79.4 kJ mol^{-1} than those of the A30P mutant-type αS in an aqueous medium. The less stable A30P mutant-type αS structures might be more reactive toward aggregation than the structures of the wild-type αS protein based on these Gibbs free energy calculations. Our thermodynamic results support our structural property findings that we describe above as well as some experiments, which predicted the oligomerization and aggregation rate of the A30P mutant-type αS protein to be increased in comparison to the wild-type αS protein.[11,12,14,20−22] Comparing the enthalpic and entropic contributions to the conformational Gibbs free energies reveals that the wild-type αS is enthalpically more preferred than the A30P mutant type by 96 kJ mol^{-1}, whereas a vice versa trend is observed for the entropic contribution (13.5 kJ mol^{-1}).

Following our previous studies with intrinsically disordered fibrillogenic proteins at the center of neurodegenerative disease,[37−40] we assessed the structural preferences of the wild-type and A30P mutant-type αS using PMF surfaces along the coordination of R_g and end-to-end distance ($R_{E\text{-}E}$) as presented in Figure 5. The PMF surfaces assess the favorability of protein conformations including solvent effects on these structures based on specific structural parameters, in this case the R_g and $R_{E\text{-}E}$ values. Due to their intrinsically disordered nature, different conformations of the αS protein may have similar thermodynamic stability, resulting in the presence of multiple basins of structures with similar thermodynamic characteristics. Determining the different structural characteristics (secondary and tertiary structures) of the conformations located in these different basins provides insights into the structural parameters that influence the stability of the wild-type and A30P mutant-type αS structures in aqueous solution. The free energy landscape of the wild-type αS shows two most favorable PMF basins (Figure 5, top). Specifically, one of the favorable PMF basins (basin IA) is located at R_g values varying between 28.0 and 35.5 Å and $R_{E\text{-}E}$ values varying between 51

dx.doi.org/10.1021/cn300198q | ACS Chem. Neurosci. 2013, 4, 486−497

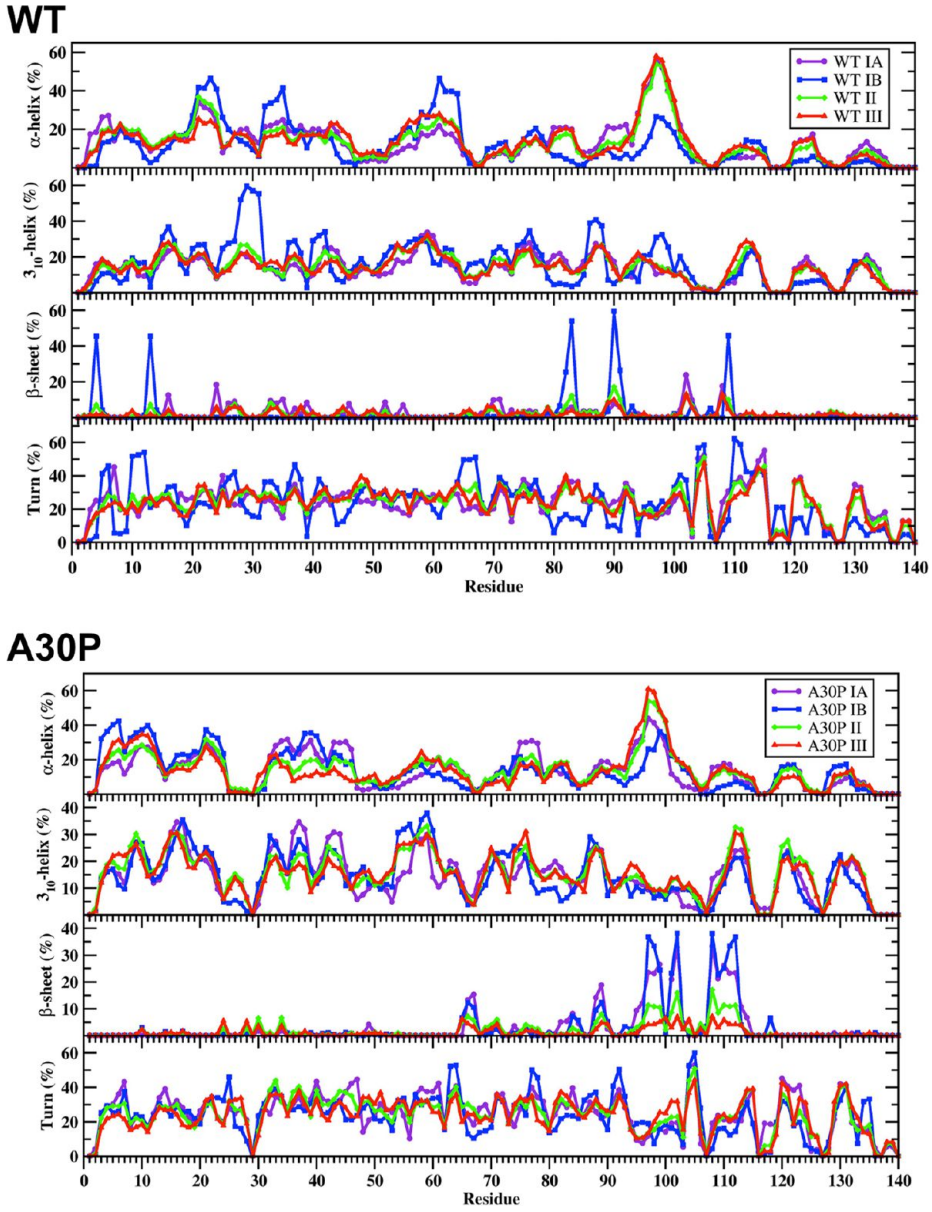

Figure 6. Wild-type and A30P mutant-type αS secondary structure components of the PMF basin structures. Calculated secondary structure abundances per residue for the structures of the wild-type (WT) and A30P mutant-type (A30P) αS located in basin IA (purple), basin IB(blue), basin II (green) and basin III (red) along the PMF surface. The abundances for the π-helix and coil structures are not displayed.

and 98 Å. The second most favorable PMF basin (basin IB) for the wild-type αS structures is located at R_g values varying between 37.4 and 42 Å and $R_{E\text{-}E}$ values varying between 108 and 148 Å. The PMF surface of the wild-type αS structures indicates that the transitions between the structures located in basin IA to basin IB or vice versa may require the overriding of large energy barriers (>1kT). The free energy landscape of the A30P mutant-type αS structures also presents two most favorable PMF basins (Figure 5, bottom). The first basin (basin IA) is located at R_g values varying between 30.5 and 36.5 Å and $R_{E\text{-}E}$ values varying between 86 and 136 Å while the second favorable basin (basin IB) is located at R_g values between 37.0 and 41.5 Å and $R_{E\text{-}E}$ values between 122 and 144 Å. Unlike the wild-type αS protein structures, transitions between the basin IA and basin IB structures of the A30P mutant-type αS protein do not require the overriding of large energy barriers.

In addition to identifying the location of the favorable basins along the PMF surfaces, the secondary and tertiary structural characteristics of the structures located in each of these basins for the wild-type and A30P mutant-type αS were calculated. The secondary structural components of each PMF basin for the wild-type and A30P mutant-type αS are presented in Figure 6. Differences in the secondary structural components of the structures in the two most favorable PMF basins (basin IA and basin IB) exist for both the wild-type and A30P mutant-type αS proteins. For the wild-type αS protein, the most abundant α-helix structure in the conformations located in basin IA occurs in the C-terminal region (Phe94-Gly101; up to 56%) but the α-helix content decreases by 30% for these residues in the structures located in basin IB. On the other side, the basin IB structures of the wild-type αS present the most abundant α-helix structure at Glu20-Val26, Lys32-Gly36, and Lys28-Thr64 in the N-terminal and NAC regions (up to 46%). The basin IA

dx.doi.org/10.1021/cn300198q | ACS Chem. Neurosci. 2013, 4, 486−497

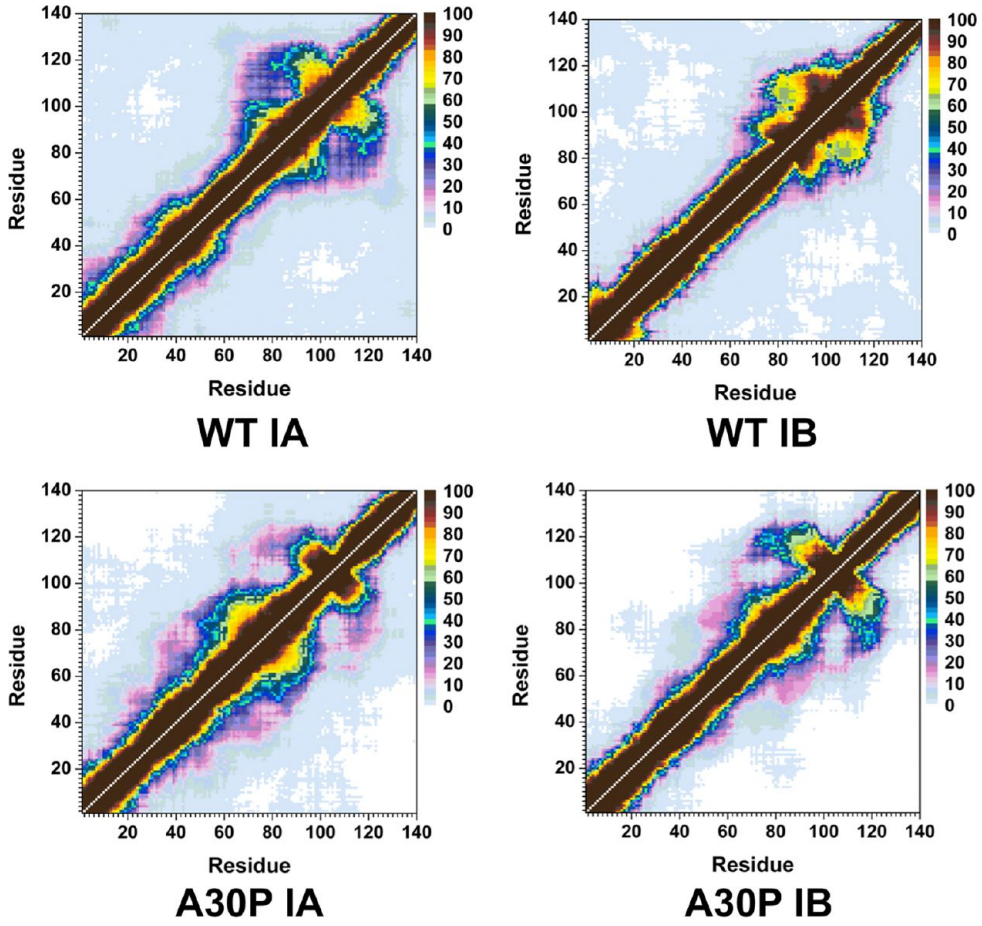

Figure 7. Wild-type and A30P mutant-type αS tertiary structures of the favorable PMF basin structures. Calculated intramolecular interactions of the wild-type αS structures located in basin IA (WT IA) and basin IB (WT IB) of the PMF surface and of the A30P mutant-type αS structures located in basin IA (A30P IA) and basin IB (A30P IB) of the PMF surface. The color scale corresponds to the probability (P) of the distance between the heavy atoms (C, N, O, S) of a residue being $\leq$20 Å from each other.

structures possess α-helix formation at these residues but with a decreased abundance than the basin IB wild-type αS structures. We also observe abundant α-helix at Met5, Lys6, Glu28, Ala29, Leu38, Val40-Lys43, Glu61, Lys80-Glu83, and Ala89-Thr92 in the N-terminal and NAC regions of the basin IA structures, whereas the basin IB structures present additional abundant α-helix formation at Leu8, Val55, Ala56, and Val77. For the A30P mutant-type αS protein, a similar trend exists in the α-helix content differences between the basin IA and basin IB structures. The basin IA structures of the A30P mutant-type αS present the most abundant α-helix formation at Phe94-Leu100 in the C-terminal region that decreases in the basin IB structures. However, the basin IB structures present the most abundant α-helix formation (up to 42%) in the N-terminal region at Val3-Glu13, whereas, the same residues in the basin IA structures form an α-helical structure with smaller. Abundant α-helical structure is also detected in the N-terminal and NAC regions at Ala19-Lys23, Lys32-Glu46, Glu61, and Thr75-Ala78 in the basin IA structures and at Val16-Gln24, Lys32-Gly41, Lys43, Thr44, Val74, and Thr75 in the basin IB structures of the A30P mutant-type αS protein.

The wild-type αS presents abundant 3_{10}-helix formation throughout the N-terminal and NAC regions as well as at a few residues in the C-terminal region for both the basin IA and basin IB structures ($\geq$20%). However, the 3_{10}-helix content is significantly increased (up to 40%) in the basin IB structures in comparison to the basin IA structures of the wild-type αS at Val15-Ala17, Gly25-Gly31, Gly36-Leu38, Val40-Ser42, Gly86-Ile88, Val95-Gln99, and Gly101. On the other hand, Lys43-Lys45, Gln79-Ala85, and Asp121-Tyr125 present the vice versa trend between the 3_{10}-helix content of the basin IA and basin IB structures of the wild-type αS protein with a difference in abundance up to 12%. The A30P mutant-type αS protein presents abundant 3_{10}-helix formation throughout the N-terminal and NAC regions as well as at residues located in the C-terminal region. However, the differences in abundance between the basin IA and basin IB structures are not as prominent as in the wild-type αS protein. Furthermore, Gly36-Leu38, Gly41-Thr44, and Val77-Glu83 present more abundant 3_{10}-helix structure in the basin IA structures in comparison to the basin IB structures of the A30P mutant-type αS. The vice versa trend is obtained for Thr54-Glu61 and Val71-Ala76 of the A30P mutant-type αS protein. Notable variations in the β-sheet formation of the wild-type and A30P mutant-type αS between the most favorable PMF basins are also observed. Specifically, the basin IA structures of the wild-type αS present abundant α-helix formation (>10%) at residues Val16, Gln24, Glu35, Val70, Val71, Lys102, and Pro108. However, the basin IB structures present abundant β-sheet structure at residues Phe4, Glu13, Val82, Glu83, Ala90, Ala91, and Gln109 with an abundance of up to 60%. In comparison, the A30P mutant-type αS presents abundant β-sheet formation at similar residues in the NAC and

dx.doi.org/10.1021/cn300198q | ACS Chem. Neurosci. 2013, 4, 486−497

C-terminal regions in both the basin IA and basin IB structures. Nevertheless, a decrease in abundance is observed for residues Gly101, Lys102, Gly111, and Ile112 in the basin IA structures in comparison to the basin IB structures.

The intramolecular interactions of the structures located in the most favorable PMF basins (basin IA and IB) of the wild-type present notable differences between the two PMF basins (Figure 6 top and bottom, respectively). Specifically, the structures of the wild-type αS located in basin IA present abundant intramolecular interactions between Gly86-Glu104 with Glu105-Ala124 and Val70-Glu83 (between 50% and 95%). In other words, abundant interactions within the NAC region and between the NAC and C-terminal regions are present in the basin IA structures of the wild-type αS. We also note interactions between the NAC region and part of the N-terminal region with the C-terminal region (up to 45%) between Val55-Gly86 and Glu104-Tyr136. Less abundant (5%) intramolecular interactions between the N-terminal (Leu8-Val16) and C-terminal (Gly132-Ala140) regions are also observed in the wild-type αS basin IA structures. Similar to the basin IA structures, abundant intramolecular interactions between the part of the NAC region and part of the C-terminal region are also detected between residues Thr72-Ile88 and Ile88-Val118 and between Ala90-Asn103 with Glu104-Pro120. However, the interactions between the NAC- and C-terminal regions with the N-terminal region (Met1-Ala18) completely disappear in the basin IB structures of the wild-type αS. Instead, we observe an increase in the abundance of intramolecular interactions within the N-terminal region between Met1-Lys10 and Gly14-Gly25 by up to 40%.

The A30P mutant-type αS structures also present significant variances in the intramolecular interactions present in the structures located in the two most favorable PMF basins (Figure 7, bottom). For example, the abundance of intramolecular interactions between Gly106-Ala124 with Val82-Lys102 increase in abundance by up to 20% in the basin IB structures in comparison to the basin IA structures of the A30P mutant-type αS. However, the opposite trend is observed for the intramolecular interactions between Thr72-Gly106 and Ala56-Thr72. Furthermore, we note a decrease in the intramolecular interactions between Val66-Val82 and Pro108-Pro128 as well as between Gln62-Ala90 and Ala29-Val52 in the basin IB structures in comparison to the basin IA structures of the A30P mutant-type αS. The less abundant interactions between residues Met1-Glu20 and the NAC region completely disappear in the basin IB structures in comparison to the basin IA structures of the A30P mutant-type αS.

The structural and thermodynamic properties of the A30P mutant-type and wild-type αS proteins reported herein indicate an increased rate of aggregation upon A30P mutation. The decrease in helicity around the A30P mutation site as well as the increase in β-sheet formation in the NAC and C-terminal regions are proposed to accelerate the oligomerization, which is an initial step in the fibrillization mechanism of αS.[29] Furthermore, the decreased long-range as well as NAC and C-terminal region intramolecular interactions upon A30P mutation are associated with an increased rate of aggregation for the A30P mutant-type rather than wild-type αS protein. The reported trends in the R_g and Gibbs free energy values of the wild-type and A30P mutant-type αS proteins further agree with a destabilized structure of the A30P mutant-type αS in comparison to the wild-type, which further is linked to the increased rate of aggregation upon A30P mutation. However, the lack of β-sheet formation in the N-terminal region of the A30P mutant-type αS protein indicates that oligomerization and/or aggregation via the N-terminal region is hindered.[29] We find that β-sheet structure formation in the NAC- and C-terminal regions is more preferred upon A30P mutation of the wild-type αS protein. These findings indicate that the oligomerization and/or aggregation tendency is larger for the A30P mutant-type αS protein due to the increased formation of β-sheet structure in these regions, which is directly linked to the reactivity in the oligomerization process. Based on these quantitative findings, our results agree with those experimental studies that reported an increased oligomerization rate for the A30P mutant-type αS in comparison to the wild-type αS.[11,12,14,15,20−23] The increased rate of oligomerization based on the structural properties at the monomeric level, suggest that the A30P mutant-type αS protein is more likely to be neurotoxic than the wild-type αS, which is in agreement with few experimental studies.[23] Our findings based on PMF surfaces of the wild-type and A30P mutant-type α-synculein indicate that both αS proteins exhibit two favorable PMF basins with different secondary and tertiary structural characteristics. However, transitions between the structures located in these two favorable PMF basins require the overriding of large energy barriers for the wild-type αS but not the A30P mutant-type αS protein. Overall, this study shows that the A30P mutation significantly impacts the structural and thermodynamic properties of the wild-type αS protein not only at the mutation site but also throughout the protein structure. Newly developed small molecules or antibodies that target the specific β-sheet forming residues in the NAC and C-terminal regions that we report in this study may hinder the formation of toxic A30P mutant-type αS oligomers. Furthermore, the information gained using our secondary structure transition stability method also provides knowledge about the most preferred secondary structure conversion resulting in the formation of the β-sheet structure for the residues located in the NAC- and C-terminal regions. From these findings, small molecules can be designed that specifically target the residues directly before the formation of a β-sheet structure at the monomeric level.

METHODS

Parallel tempering or replica exchange molecular dynamics (REMD) simulations utilize several replicas at different temperatures that exchange throughout the course of the simulation in order to allow the sampling of different minimum energy conformations within the same simulation, unlike classical MD.[47] As a result, REMD simulations provide enhanced conformational sampling of protein structures, which is a necessity for simulations of intrinsically disordered proteins.[47,48] Therefore, we performed REMD simulations on the full length wild-type and A30P mutant-type αS proteins using the Onufriev−Bashford−Case generalized Born implicit solvent model.[47,49] An implicit solvent model was used in order to prevent errors due to confined aqueous volume or nonconstant heat capacity in explicit water REMD simulations.[37,38] The REMD simulations were performed with the AMBER 11 software package along with Amber ff99SB potential functions for the protein.[50,51] A total number of 56 replicas were utilized with temperatures exponentially distributed between 283 and 490 K.[52] The initial structures were equilibrated for 500 ns for each replica with a time step of 2 fs. Each replica was then simulated for a total of 40 ns with exchanges attempted every 5 ps while trajectories were saved every 500 steps. Langevin dynamics with a collision frequency of 2 ps^{-1} was used to control the temperature.[53,54] The particle mesh Ewald method with a cutoff value of 450 Å was used to treat the long-range interactions, and bonds were constrained using the SHAKE algorithm.[53,54] Based on the cumulative

dx.doi.org/10.1021/cn300198q | ACS Chem. Neurosci. 2013, 4, 486−497

secondary structure abundance,[37,38] we concluded that both the wild-type and A30P mutant-type αS simulations reached convergence after 20 ns of simulation per replica (see the Supporting Information). The structural and thermodynamic properties of the structures obtained after convergence were calculated for the replica closest to physiological temperature (310 K). The DSSP program, which incorporates hydrogen bond criteria, was used to analyze the secondary structure components of the wild- and A30P mutant-type αS.[55] In addition, the stability of residual secondary structure transitions of the wild-type and A30P mutant-type αS was assessed using our recently published theoretical strategy.[39,40] Intramolecular interactions were considered to occur if at least one heavy atom (C, O, N, S) of a specific residue was at least $\leq$20 Å from the heavy atom of another residue. A cutoff distance of 20 Å was utilized in order to account for any long-range intramolecular interactions observed experimental from residual dipolar coupling measurements. Thermodynamic analysis was performed on the 20 000 structures obtained after convergence for both the wild-type and A30P mutant-type αS using the molecular mechanics/Poisson−Boltzmann surface area (MM/PBSA) method and potential mean force (PMF) calculations.[37,38,56,57] The PMF calculations were based on coordinates of end-to-end distance ($R_{E\text{-}E}$), which is the distance between the N-terminus backbone N atom and the C-terminus backbone carboxyl O atom, and radius of gyration (R_g) as in our previous studies with intrinsically disordered fibrillogenic peptides.[37,38] The thermodynamic calculations utilizing the MM/PBSA method used dielectric constant values of 1 and 80 for the protein and solvent environment, respectively. Furthermore, the entropy values were estimated using the normal-mode analysis (NMA).[58] Quasi-harmonic entropy calculations using the Schlitter method were attempted,[59] however, the conformational variances were too large to be handled using this method.

■ ASSOCIATED CONTENT

Supporting Information

Convergence figures for the wild-type and A30P mutant-type αS. Cconvergence figures for the secondary structure transition stabilities and the PMF surfaces of both peptides. Description of tertiary structural properties of both peptides for the least favorable basins on the PMF surfaces. This material is available free of charge via the Internet at http://pubs.acs.org.

■ AUTHOR INFORMATION

Corresponding Author

*E-mail: orkid.coskuner@utsa.edu.

Author Contributions

O.C. designed the research and simulations. A.A. and O.W.-S. performed the simulations. O.C. developed the secondary structure transition strategy and O.W.-S. coded the developed secondary structure transition software. A.D., A.A., and I.S. assisted O.C. and O.W.-S. in writing the paper.

Funding

This research was supported by an allocation and computing resources provided by the National Science Foundation (Grant No. TG-CHE110044). The authors are thankful for the financial support from the University of Texas at San Antonio.

Notes

The authors declare no competing financial interest.

■ ACKNOWLEDGMENTS

The calculations and simulations were performed on Kraken at the National Institute for Computational Sciences, Texas Advanced Computing Center (TACC) and the Computational Biology Initiative and The University of Texas at San Antonio. We thank Dr. George Perry for reading the manuscript.

■ ABBREVIATIONS

αS α-synuclein; far-UV-CD far-ultraviolet-circular dichroism; SMF single molecule force; FTIR Fourier transform infrared; FRET Förster resonance energy transfer; NAC non-amyloid-β component; SDS sodium dodoceyl sulfate; REMD replica exchange molecular dynamics; NMR nuclear magnetic resonance; R_g radius of gyration; R_{E-E} end-to-end distance; PMF potential of mean force; MM/PBSA Molecular Mechanics/Poisson−Boltzmann surface area; NMA normal-mode analysis

■ REFERENCES

(1) Spillantini, M. G., Schmidt, M. L., Lee, V. M. Y., Trojanowski, J. Q., Jakes, R., and Goedert, M. (1997) alpha-synuclein in Lewy bodies. *Nature 388*, 839−840.

(2) Clayton, D. F., and George, J. M. (1998) The synucleins: a family of proteins involved in synaptic function, plasticity, neurodegeneration and disease. *Trends Neurosci. 21*, 249−254.

(3) Kruger, R., Muller, T., and Riess, O. (2000) Involvement of alpha-synuclein in Parkinson's disease and other neurodegenerative disorders. *J. Neural Transm. 107*, 31−40.

(4) Maroteaux, L., Campanelli, J. T., and Scheller, R. H. (1988) Synuclein - A Neuron-specific protein localized to the nucleus and presynaptic nerve-terminal. *J. Neurosci. 8*, 2804−2815.

(5) Polymeropoulos, M. H., Higgins, J. J., Golbe, L. I., Johnson, W. G., Ide, S. E., DiIorio, G., Sanges, G., Stenroos, E. S., Pho, L. T., Schaffer, A. A., Lazzarini, A. M., Nussbaum, R. L., and Duvoisin, R. C. (1996) Mapping of a gene for Parkinson's disease to chromosome 4q21-q23. *Science 274*, 1197−1199.

(6) Goedert, M. (2001) Parkinson's disease and other alpha-synucleinopathies. *Clin. Chem. Lab. Med. 39*, 308−312.

(7) Singleton, A. B., Farrer, M., Johnson, J., Singleton, A., Hague, S., Kachergus, J., Hulihan, M., Peuralinna, T., Dutra, A., Nussbaum, R., Lincoln, S., Crawley, A., Hanson, M., Maraganore, D., Adler, C., Cookson, M. R., Muenter, M., Baptista, M., Miller, D., Blancato, J., Hardy, J., and Gwinn-Hardy, K. (2003) alpha-synuclein locus triplication causes Parkinson's disease. *Science 302*, 841−841.

(8) Kruger, R., Kuhn, W., Muller, T., Woitalla, D., Graeber, M., Kosel, S., Przuntek, H., Epplen, J. T., Schols, L., and Riess, O. (1998) Ala30Pro mutation in the gene encoding alpha-synuclein in Parkinson's disease. *Nat. Genet. 18*, 106−108.

(9) Polymeropoulos, M. H., Lavedan, C., Leroy, E., Ide, S. E., Dehejia, A., Dutra, A., Pike, B., Root, H., Rubenstein, J., Boyer, R., Stenroos, E. S., Chandrasekharappa, S., Athanassiadou, A., Papapetropoulos, T., Johnson, W. G., Lazzarini, A. M., Duvoisin, R. C., DiIorio, G., Golbe, L. I., and Nussbaum, R. L. (1997) Mutation in the alpha-synuclein gene identified in families with Parkinson's disease. *Science 276*, 2045−2047.

(10) Zarranz, J. J., Alegre, J., Gomez-Esteban, J. C., Lezcano, E., Ros, R., Ampuero, I., Vidal, L., Hoenicka, J., Rodriguez, O., Atares, B., Llorens, V., Tortosa, E. G., del Ser, T., Munoz, D. G., and de Yebenes, J. G. (2004) The new mutation, E46K, of alpha-synuclein causes Parkinson and Lewy body dementia. *Ann. Neurol. 55*, 164−173.

(11) Li, J., Uversky, V. N., and Fink, A. L. (2002) Conformational behavior of human alpha-synuclein is modulated by familial Parkinson's disease point mutations A30P and A53T. *Neurotoxicology 23*, 553−567.

(12) Li, J., Uversky, V. N., and Fink, A. L. (2001) Effect of familial Parkinson's disease point mutations A30P and A53T on the structural properties, aggregation, and fibrillation of human alpha-synuclein. *Biochemistry 40*, 11604−11613.

(13) Volles, M. J., Lee, S. J., Rochet, J. C., Shtilerman, M. D., Ding, T. T., Kessler, J. C., and Lansbury, P. T. (2001) Vesicle permeabilization by protofibrillar alpha-synuclein: Implications for the pathogenesis and treatment of Parkinson's disease. *Biochemistry 40*, 7812−7819.

(14) Conway, K. A., Lee, S. J., Rochet, J. C., Ding, T. T., Williamson, R. E., and Lansbury, P. T. (2000) Acceleration of oligomerization, not

fibrillization, is a shared property of both alpha-synuclein mutations linked to early-onset Parkinson's disease: Implications for pathogenesis and therapy. *Proc. Natl. Acad. Sci. U.S.A. 97*, 571−576.
(15) Conway, K. A., Harper, J. D., and Lansbury, P. T. (1998) Accelerated in vitro fibril formation by a mutant alpha-synuclein linked to early-onset Parkinson disease. *Na. Med. 4*, 1318−1320.
(16) El-Agnaf, O. M. A., Jakes, R., Curran, M. D., and Wallace, A. (1998) Effects of the mutations Ala(30) to Pro and Ala(53) to Thr on the physical and morphological properties of alpha-synuclein protein implicated in Parkinson's disease. *FEBS Lett. 440*, 67−70.
(17) Giasson, B. I., Uryu, K., Trojanowski, J. Q., and Lee, V. M. Y. (1999) Mutant and wild type human alpha-synucleins assemble into elongated filaments with distinct morphologies in vitro. *J. Biol. Chem. 274*, 7619−7622.
(18) Serpell, L. C., Berriman, J., Jakes, R., Goedert, M., and Crowther, R. A. (2000) Fiber diffraction of synthetic alpha-synuclein filaments shows amyloid-like cross-beta conformation. *Proc. Natl. Acad. Sci. U.S.A. 97*, 4897−4902.
(19) Cho, M. K., Kim, H. Y., Fernandez, C. O., Becker, S., and Zweckstetter, M. (2011) Conserved core of amyloid fibrils of wild type and A30P mutant alpha-synuclein. *Protein Sci. 20*, 387−395.
(20) Lashuel, H. A., Petre, B. M., Wall, J., Simon, M., Nowak, R. J., Walz, T., and Lansbury, P. T. (2002) alpha-synuclein, especially the Parkinson's disease-associated mutants, forms pore-like annular and tubular protofibrils. *J. Mol. Biol. 322*, 1089−1102.
(21) Kamiyoshihara, T., Kojima, M., Ueda, K., Tashiro, M., and Shimotakahara, S. (2007) Observation of multiple intermediates in alpha-synuclein fibril formation by singular value decomposition analysis. *Biochem. Biophys. Res. Commun. 355*, 398−403.
(22) Narhi, L., Wood, S. J., Steavenson, S., Jiang, Y. J., Wu, G. M., Anafi, D., Kaufman, S. A., Martin, F., Sitney, K., Denis, P., Louis, J. C., Wypych, J., Biere, A. L., and Citron, M. (1999) Both familial Parkinson's disease mutations accelerate alpha-synuclein aggregation. *J. Biol. Chem. 274*, 9843−9846.
(23) Winner, B., Jappelli, R., Maji, S. K., Desplats, P. A., Boyer, L., Aigner, S., Hetzer, C., Loher, T., Vilar, M., Campionic, S., Tzitzilonis, C., Soragni, A., Jessberger, S., Mira, H., Consiglio, A., Pham, E., Masliah, E., Gage, F. H., and Riek, R. (2011) In vivo demonstration that alpha-synuclein oligomers are toxic. *Proc. Natl. Acad. Sci. U.S.A. 108*, 4194−4199.
(24) Ono, K., Ikeda, T., Takasaki, J., and Yamada, M. (2011) Familial Parkinson disease mutations influence alpha-synuclein assembly. *Neurobiol. Dis. 43*, 715−724.
(25) Choong, C. J., and Say, Y. H. (2011) Neuroprotection of alpha-synuclein under acute and chronic rotenone and maneb treatment is abolished by its familial Parkinson's disease mutations A30P, A53T and E46K. *Neurotoxicology 32*, 857−863.
(26) Moussa, C. E. H., Wersinger, C., Tomita, Y., and Sidhu, A. (2004) Differential cytotoxicity of human wild type and mutant alpha-synuclein in human neuroblastoma SH-SY5Y cells in the presence of dopamine. *Biochemistry 43*, 5539−5550.
(27) Wersinger, C., and Sidhu, A. (2003) Differential cytotoxicity of dopamine and H2O2 in a human neuroblastoma divided cell line transfected with alpha-synuclein and its familial Parkinson's disease-linked mutants. *Neurosci. Lett. 342*, 124−128.
(28) Bertoncini, C. W., Fernandez, C. O., Griesinger, C., Jovin, T. M., and Zweckstetter, M. (2005) Familial mutants of alpha-synuclein with increased neurotoxicity have a destabilized conformation. *J. Biol. Chem. 280*, 30649−30652.
(29) Bussell, R., and Eliezer, D. (2001) Residual structure and dynamics in Parkinson's disease-associated mutants of alpha-synuclein. *J. Biol. Chem. 276*, 45996−46003.
(30) Brucale, M., Sandal, M., Di Maio, S., Rampioni, A., Tessari, I., Tosatto, L., Bisaglia, M., Bubacco, L., and Samori, B. (2009) Pathogenic Mutations Shift the Equilibria of alpha-Synuclein Single Molecules towards Structured Conformers. *ChemBioChem 10*, 176−183.
(31) Ferreon, A. C. M., Moran, C. R., Ferreon, J. C., and Deniz, A. A. (2010) Alteration of the alpha-Synuclein Folding Landscape by a Mutation Related to Parkinson's Disease. *Angew. Chem., Int. Ed. 49*, 3469−3472.
(32) Jo, E. J., Fuller, N., Rand, R. P., St George-Hyslop, P., and Fraser, P. E. (2002) Defective membrane interactions of familial Parkinson's disease mutant A30P alpha-synuclein. *J. Mol. Biol. 315*, 799−807.
(33) Losasso, V., Pietropaolo, A., Zannoni, C., Gustincich, S., and Carloni, P. (2011) Structural Role of Compensatory Amino Acid Replacements in the alpha-Synuclein Protein. *Biochemistry 50*, 6994−7001.
(34) Chatterjee, P., and Sengupta, N. (2012) Effect of the A30P mutation on the structural dynamics of micelle-bound alpha Synuclein released in water: a molecular dynamics study. *Eur. Biophys. J. Biophys. Lett. 41*, 483−489.
(35) Balesh, D., Ramjan, Z., and Floriano, W. B. (2011) Unfolded annealing molecular dynamics conformers for wild-type and disease-associated variants of alpha-synuclein show no propensity for beta-sheet formation. *J. Biophys. Chem. 2*, 123−133.
(36) Perlmutter, J. D., Braun, A. R., and Sachs, J. N. (2009) Curvature Dynamics of alpha-Synuclein Familial Parkinson Disease Mutants Molecular Simulations of the Micelle- and Bilayer-Bound Forms. *J. Biol. Chem. 284*, 7177−7189.
(37) Wise-Scira, O., Xu, L., Kitahara, T., Perry, G., and Coskuner, O. (2011) Amyloid-beta peptide structure in aqueous solution varies with fragment size, *J. Chem. Phys. 135*.
(38) Wise-Scira, O., Xu, L., Perry, G., and Coskuner, O. (2012) Structures and free energy landscapes of aqueous zinc(II)-bound amyloid-beta(1−40) and zinc(II)-bound amyloid-beta(1−42) with dynamics. *J. Biol. Inorg. Chem. 17*, 927−938.
(39) Coskuner, O., Wise-Scira, O., Perry, G., and Kitahara, T. (2012) The Structures of the E22Δ Mutant-Type Amyloid-β Alloforms and the Impact of E22Δ Mutation on the Structures of the Wild-Type Amyloid-β Alloforms. *ACS Chem. Neurosci.* DOI: 10/1021/cn300149j.
(40) Wise-Scira, O., Dunn, A., Aloglu, A. K., Sakallioglu, I. T., and CoskunerO. (2013) Structures of the E46K Mutant-Type α-Synuclein Protein and Impact of E46K Mutation on the Structures of the Wild-Type α-Synuclein Protein. *ACS Chem. Neurosci.*, in press.
(41) Barrow, C. J., and Zagorski, M. G. (1991) Solution Structures of Beta Peptide and Its Constituent Fragments - Relation to Amyloid Deposition. *Science 253*, 179−182.
(42) Kessler, J. C., Rochet, J. C., and Lansbury, P. T. (2003) The N-terminal repeat domain of alpha-synuclein inhibits beta-sheet and amyloid fibril formation. *Biochemistry 42*, 672−678.
(43) Kim, Y. S., Lim, D., Kim, J. Y., Kang, S. J., Kim, Y.-H., and Im, H. (2009) beta-Sheet-breaking peptides inhibit the fibrillation of human alpha-synuclein. *Biochem. Biophys. Res. Commun. 387*, 682−687.
(44) Bertoncini, C. W., Jung, Y. S., Fernandez, C. O., Hoyer, W., Griesinger, C., Jovin, T. M., and Zweckstetter, M. (2005) Release of long-range tertiary interactions potentiates aggregation of natively unstructured alpha-synuclein. *Proc. Natl. Acad. Sci. U.S.A. 102*, 1430−1435.
(45) Giasson, B. I., Murray, I. V. J., Trojanowski, J. Q., and Lee, V. M. Y. (2001) A hydrophobic stretch of 12 amino acid residues in the middle of alpha-synuclein is essential for filament assembly. *J. Biol. Chem. 276*, 2380−2386.
(46) Lee, J. C., Langen, R., Hummel, P. A., Gray, H. B., and Winkler, J. R. (2004) alpha-synuclein structures from fluorescence energy-transfer kinetics: Implications for the role of the protein in Parkinson's disease. *Proc. Natl. Acad. Sci. U.S.A. 101*, 16466−16471.
(47) Sugita, Y., and Okamoto, Y. (1999) Replica-exchange molecular dynamics method for protein folding. *Chem. Phys. Lett. 314*, 141−151.
(48) Zhang, W., Wu, C., and Duan, Y. (2005) Convergence of replica exchange molecular dynamics. *J. Chem. Phys. 123*, 154105.
(49) Case, D. A., Onufriev, A., and Bashford, D. (2004) Exploring protein native states and large-scale conformational changes with a modified generalized born model. *Proteins 55*, 383−394.
(50) Case, D., Darden, T., Cheatham, T., Simmerling, C., Wang, J., Duke, R., Luo, R., Walker, R., Zhang, W., and Merz, K. (2010) *AMBER 11*, University of California, San Francisco.

(51) Hornak, V., Abel, R., Okur, A., Strockbine, B., Roitberg, A., and Simmerling, C. (2006) Comparison of multiple amber force fields and development of improved protein backbone parameters. *Proteins 65*, 712−725.
(52) van der Spoel, D., and Patriksson, A. (2008) A temperature predictor for parallel tempering simulations. *Phys. Chem. Chem. Phys. 10*, 2073−2077.
(53) Allen, M. P., and Tildesley, D. J. (1999) *Computer simulation of liquids*, Clarendon Press: Oxford.
(54) Frenkel, D., and Smit, B. (2002) *Understanding molecular simulation: from algorithms to applications*, Vol. *1*, Academic Press: San Diego, CA.
(55) Kabsch, W., and Sander, C. (1983) Dictionary of Protein Secondary Structure - Pattern-Recognition of Hydrogen-Bonded and Geometrical Features. *Biopolymers 22*, 2577−2637.
(56) Lee, M. R., Duan, Y., and Kollman, P. A. (2000) Use of MM-PB/SA in estimating the free energies of proteins: Application to native, intermediates, and unfolded villin headpiece. *Proteins: Struct., Funct., Genet. 39*, 309−316.
(57) Kollman, P. A., Massova, I., Reyes, C., Kuhn, B., Huo, S. H., Chong, L., Lee, M., Lee, T., Duan, Y., Wang, W., Donini, O., Cieplak, P., Srinivasan, J., Case, D. A., and Cheatham, T. E. (2000) Calculating structures and free energies of complex molecules: Combining molecular mechanics and continuum models. *Acc. Chem. Res. 33*, 889−897.
(58) Case, D. A. (1994) Normal-Mode Analysis of Protein Dynamics. *Curr. Opin. Struct. Biol. 4*, 285−290.
(59) Schlitter, J. (1993) Estimation of Absolute and Relative Entropies of Macromolecules Using the Covariance-Matrix. *Chem. Phys. Lett. 215*, 617−621.
(60) Kumar, S., Sarkar, A., and Sundar, D. (2009) Controlling the aggregation propensity in A53T mutant of alpha-synuclein causing Parkinson's Disease. *Biochem. Biophys. Res. Comm. 387*, 305−309.